

# Internal Structures in Fluid Beds of Different Scales: An Application of Electrical Capacitance Tomography.

R B White and A Zakhari

CSIRO Minerals, Bayview Avenue, Clayton, Victoria 3169, AUSTRALIA  
Email: r.white@minerals.csiro.au

**Abstract** – *Electrical capacitance tomographic imaging has been used to investigate the behaviour of smelter grade alumina in 200 mm, 300 mm and 600 mm ID fluid beds. Internal structures resulting from gas-solid interaction have been identified in each fluid bed. The scale of operation can be seen to influence the way the structures form and move through the bed, and these observations may account for the difficulty in modelling fluid bed behaviour at different scales of operation. Some aspects of the internal structures, such as the general size at a particular operating condition, can be seen to be relatively consistent in the different scale fluid beds.*

**Keywords:** fluid bed, capacitance tomography

## 1 INTRODUCTION

Fluid beds are widely used in the process industries as reactors to contact gases and solids. Many different processes have been developed over the past 50 years around the fluid bed, such as the roasting of mineral ores and the upgrading of oil in the petrochemical industry. The term "fluid bed" has also come to encompass a range of reactors to enable the contact of gas and solids, and fluid beds can operate over a wide velocity range. The gas is usually introduced at the base of the reactor, and at low gas velocity "bubbles" of gas rise through a bed of solids in the **bubbling fluidised bed**. As the gas velocity is increased, solids begin to be entrained from the surface of the bed and can be swept out of the reactor with the fluidising gas. The amount of solids leaving the bed surface can increase rapidly as higher gas velocities are used and the bed of solids can quickly be depleted. A **circulating fluidised bed**, which operates at higher gas velocities, incorporates components to separate the entrained solids from the exiting gas stream and re-introduce them to the base of the reactor for repeated contact with the fluidising gas stream.

Process development for a fluid bed process is often expensive because of the lack of a highly developed model to predict in detail how the gas and solid will interact. Several different fluid beds are usually built and operated to obtain reaction data at increasing scales of operation because it is well known that the internal characteristics of the gas-solid interaction change with scale of operation.

Electrical Capacitance Tomography (ECT) is being used to investigate internal structures in fluid beds. Halow [1] developed a system to investigate the internal structures in a 150 mm inside diameter (ID) bubbling fluidised bed in the 1980's and has recently developed a model to show bubble movement in the system [2]. An ECT system developed at UMIST, UK, was used by Wang [3] to investigate bubble growth near the base of a 150 mm ID bubbling fluidised bed. This ECT system was commercialised by PTL, UK, and the results of several investigations using the system have been reported in the literature. White [4] compared the behaviour of several different types of solids in a 200 mm ID bubbling fluidised bed and reported reasonable agreement with a bubble growth correlation from the literature. Mathers [5] investigated the behaviour near the centre of a 300 mm ID, conical based fluid bed with a bed depth of 1300 mm operating at intermediate gas velocities. Rhodes [6] has investigated the solids distribution the lean-phase region high in a 90 mm ID circulating fluidised bed, and White [7] has investigated the dense-phase region near the base of a 200 mm ID circulating fluidised bed as the gas velocity is changed over a wide range.

## 2 EQUIPMENT

A PTL-200 ECT system has been used in this study to investigate the solids distribution in a 200 mm, 300 mm and a 600 mm ID fluid bed of smelter grade alumina. The 200 mm and 300 mm ID beds were both constructed of clear PVC. In the 200 mm ID bed 12 electrodes, each 75 mm high and 50 mm wide, were attached to the outside of the PVC wall. Inter-electrode shields of 2 mm were installed between the 125 mm high

earthing collars, which were installed above and below the measurement electrodes. In the 300 mm ID bed 12 electrodes were also attached to the outside of the PVC wall, and each electrode was 152 mm high and 76 mm wide. Inter-electrode shields of 1 mm were used and the earthing collars were 152 mm high. A rigid earth shield was installed on each fluid bed test section that was spaced 12 mm above the electrodes and extended the whole length of the electrodes and earthing collars. The 600 mm ID bed was constructed of mild steel and the 8 electrodes, each 148 mm high and 210 mm wide, were mounted on the inside of the fluid bed. Each electrode was mounted on a rigid PVC foam spacer, and the hook-up cables were passed through holes drilled through the steel wall.

The 200 mm ID bed was fluidised with dry nitrogen and operated in two different configurations: as a 400 mm deep bed with the ECT sensor centred 200 mm above the base, and with a 600 mm deep bed with the ECT sensor centred 400 mm above the base. The 300 mm ID bed was fluidised with dry nitrogen, the ECT sensor was centred 300 mm above the base and the bed of smelter grade alumina was 600 mm deep. The 600 mm ID fluid bed was also 600 mm deep, but was fluidised with air and the ECT sensor was centred 300 mm above the bed floor. The bed material in all fluid beds was taken from the same batch of smelter grade alumina, with particle size of 0.130 mm, particle density of 3.33 g/ml and tapped, bulk density of 1.09 g/ml.

### 3 METHOD

The PTL-200 ECT system is a transputer based system and was supplied with integrated software to calibrate the sensors and either view reconstructed images in real-time on a dedicated monitor, or to log measurements to hard disk for off-line analysis. Software was supplied by PTL to process the logged measurement files and generate series of reconstructed images using the linear back projection algorithm. Each reconstructed image is presented as an array of 32 elements by 32 elements, where the value in each element corresponds to the local solids fraction in a particular region in the measurement volume and lies in the range of 0 to 1. The ECT system attached to the fluid beds was calibrated before the test runs and the value 1 represents the solids concentration encountered when the measurement volume is filled with well settled, or packed, smelter grade alumina. The value 0 represents the condition when only fluidising gas is present in the measurement volume.

An array of reconstructed images has been plotted to represent 5 seconds of real time operation at a range of gas velocities for each fluid bed. Iso-surfaces have been plotted to

enclose regions where solids fractions are less than 0.2, 0.5 and 0.8, and each region can be identified in the plot. Since the vertical, Z, axis in the plot is time, the plot appears to show a possible route taken by each region as it travels upwards through the bed. In reality only consecutive measurements taken at the sensor location are plotted in these bed fraction plots.

The plots showing 5 seconds of operation in the 200 mm and 300 mm ID fluid beds contain 500 reconstructed images, while the plots showing behaviour in the 600 mm ID fluid bed contain 1175 reconstructed images, and were generated using the plotting package T3D, by Fortner software. The lightest shading encloses a region where the solids fraction  $\leq 0.8$ , the medium shading encloses a region where solids fraction  $\leq 0.5$  and the darkest shading encloses the region where solids fraction  $\leq 0.2$ .

It should be noted that the fluid bed generally provides a good mixing environment for gas and solids because of the upward movement of gas and the downward movement of the solids, [8]. The region where solids fraction  $> 0.8$ , outside the lightest shaded region, can be considered as the region where the downward movement of solids in a condition close to that of a packed bed occurs. Inside the regions defined by the iso-surfaces the bed material is expanded by fluidising gas, and the region where solids fraction  $\leq 0.2$  can be thought of as essentially a gas bubble, although White, [7], discusses this type of classification in considerably more detail.

### 4 RESULTS AND DISCUSSION

Fluidisation experiments were carried out over a range of gas velocities and the ECT system was used to measure solids concentration in the measurement volume. Iso-surface plots, showing the bed fraction occupied by regions where bed material has been expanded by fluidising gas, have been constructed at each test condition. Figure 1 shows results from the 400 mm deep bed in the 200 mm ID test section, where the onset and establishment of bubbles in a fluidised bed can be seen. Figure 2 shows bubble development in the 300 mm ID test section operated with a 600 mm deep bed, and the regions can be seen to rise almost vertically to the bed surface. Figure 3 shows bubble development in the 600 mm ID test section with a bed depth of 600 mm, and it should be noted that the gas velocities used are approximately one order of magnitude higher than those required to form bubbles in the 200 mm ID fluid bed. Figure 4 shows results from the 600 mm deep 200 mm ID fluid bed operated over a very wide gas velocity range, and it should be noted that the ECT sensor is centred 400 mm from the base of the bed. These results are discussed in greater detail elsewhere, [9], and essentially show the

changes in internal structure that occur as the gas velocity is increased and the bubbling fluidised bed transforms into a circulating fluidised bed.

#### 4.1 200 mm ID fluid bed with 400 mm deep bed

Regions of expanded bed material, where solids fraction  $\leq 0.8$ , can be seen distributed throughout the solids in the measurement volume at a gas velocity,  $u$ , of 0.035 m/s, see Figure 1.

At  $u = 0.05$  m/s near  $Z = 173, 434$  and  $495$  small regions of more highly expanded bed material, where solids fraction  $\leq 0.5$ , can be seen to form and grow as the gas velocity is increased.

At  $u = 0.06$  m/s a characteristic internal structure can be seen to form near  $Z = 124$  and  $Z = 173$ . The structure consists of a small region where of solids fraction  $\leq 0.2$  – a bubble - existing inside a larger region enclosed by the other iso-surface contours. The observation that considerable expansion of the fluid bed occurs before discrete bubbles are formed is a well known characteristic of this type of solid, a Group A solid, [10].

#### 4.2 300 mm ID fluid bed with 600 mm deep bed

Regions of expanded bed material, where solids fraction  $\leq 0.8$  can be seen in the fluid bed at a gas velocity,  $u$ , of 0.033 m/s, see Figure 2. These regions have a similar diameter as those identified at similar conditions in the 200 mm ID fluid bed, but do not appear to be evenly distributed throughout the solids in the measurement volume. (A direct measurement of the feature size presented in the Figures 1 and 2 cannot be made because a different scaling factor is used in each figure.)

Structures appear to grow at approximately the same rate in the 300 mm ID bed and the 200 mm ID bed. The region where solids fraction  $\leq 0.5$  at  $u = 0.049$  m/s at  $Z = 74$  in Figure 2 is similar in size to the region in Figure 1 at  $u = 0.05$  m/s near  $Z = 160$ . The expanded region in the 300 mm ID fluid bed appears to be more continuous than in the 200 mm ID bed at these gas velocities and the fluidising gas rises as a persistent column through the 300 mm ID fluid bed.

At  $u = 0.07$  m/s, the occasional region where the solids fraction is  $\leq 0.2$  can be seen in both the 300 mm ID and 200 mm ID fluid beds, but it appears that the diameter of the region may be up to 50% greater in the smaller fluid bed. The region seen at  $Z = 371$  in Figure 2 is significantly smaller than the region seen at  $Z = 124$  in Figure 1. The size of the other regions, where the solids fraction is  $\leq 0.8$  which enclose regions where solids fraction is  $\leq 0.5$ , are in good agreement

between the 300 mm ID and 200 mm ID fluid beds.

The general observation is that gas rises through the 300 mm ID bed much more continuously than in the 200 mm ID fluid bed, but the regions where the solids fraction  $\leq 0.5$  are generally of similar diameter in both beds. There is some evidence that the region with solids fraction  $\leq 0.2$  may be larger in the 200 mm ID bed than in the 300 mm ID bed and occur more frequently at the same gas velocity.

#### 4.3 600 mm ID fluid bed with 600 mm deep bed

Flow rates of the fluidising air could not be adjusted low enough to directly compare operation at the same gas velocities as investigated in the smaller fluid beds, and the lowest gas velocity achievable was 0.5 m/s. At this velocity, however, no regions where solids fraction  $\leq 0.2$  or solids fraction  $\leq 0.5$  were observed, but regions of expanded bed material, where solids fraction  $\leq 0.8$ , are distributed throughout the solids in the measurement volume, see Figure 3. In the 200 mm ID fluid bed operating at this velocity, regions where solids fraction  $\leq 0.5$  are seen to frequently occupy  $> 75\%$  of the whole bed cross-section, and regions where solids fraction is  $\leq 0.2$  are also occasionally seen (eg near  $Z = 198$ ), as shown in Figure 4.

Regions with solids fraction  $\leq 0.5$  can be detected passing through the measurement volume at  $u = 0.61$  m/s. These regions appear to be approximately the same size as those seen in the 200 mm ID fluid bed at this gas velocity, but appear less frequently. Near  $Z = 718$  a region with solids fraction  $\leq 0.5$  can be seen to rise near vertically alongside a large region with solids fraction  $\leq 0.8$ . Near  $Z = 347$  it appears that 2 regions with solids fraction  $\leq 0.5$  rise rapidly side-by-side, and at  $Z = 842$  several regions with solids fraction  $\leq 0.5$  rise more slowly together.

As the gas velocity is increased, regions with solids fraction  $\leq 0.5$  appear more frequently. Near  $Z = 668$  and  $Z = 1015$  at  $u = 0.66$  m/s regions with solids fraction  $\leq 0.5$  appear to rise through the fluid bed at an angle of approximately  $45^\circ$ . This observation is particularly interesting because it would indicate a mechanism for the high lateral velocity detected using tracer particles at the surface of a large fluid bed operating with a different bed material, [11].

The first bubble can be seen at  $u = 0.86$  m/s near  $Z = 569$ , and appears to exist inside an extensive region where solids fraction  $\leq 0.5$ , as shown in Figure 3. This bubble is nearly twice the diameter of the bubbles seen near  $Z = 25$  and  $Z = 248$  at  $u = 0.9$  in the 200 mm ID fluid bed, see Figure 4. It is reasonable to assume that at this

gas velocity the bubble size in the small bed is strongly influenced by the presence of the walls.

It is interesting that all the bubbles in the small bed are contained within significantly larger regions where solids fraction gradually increases to 0.8, but in the large bed a bubble can be seen at  $u = 0.95$  m/s near  $Z = 173$ , as shown in Figure 3. These observations suggest that bubbles can exist in forms in the large fluid bed and supports some observations of unexpected bubble behaviour made using X-ray imaging in a small fluid bed, [12].

## 5 CONCLUSIONS

- Electrical capacitance tomographic imaging can be used to investigate the internal behaviour of 200 mm, 300 mm and 600 mm ID fluid beds of smelter grade alumina.
- Internal features can be identified in each size fluid bed using ECT.
- Some aspects of the behaviour of the internal features is consistent with previously well known behaviour, such as bed expansion at low gas velocity.
- Some differences in the behaviour of the internal features of large and small fluid beds support previously reported behaviour, such as oblique movement of bed material in the large bed that would result in a high lateral solids velocity in the large bed [11], and the presence of different forms of bubbles [12].
- Differences in the behaviour of the internal features of large and small fluid beds, such as the layers of expanded bed material surrounding a bubble in the small fluid bed, the formation of multiple regions of expanded bed material in the largest fluid bed and the likely suppression of bubble growth in the small bed. It is unlikely that these observed differences in behaviour result from a difference in spatial resolution in the different scale fluid beds, but additional sensor development is in progress to install a 12 sensor array in the 600 mm ID fluid bed.
- The scale of operation influences the formation and behaviour of internal structures and may be responsible for the difficulty in modelling gas solid interaction to predict performance at different scales of operation.

## 6 ACKNOWLEDGEMENTS

The authors would like to thank the Cooperative Research Centre for New Technologies for Power Generation from Low-

Rank Coals for the use of the process tomography equipment.

## 7 REFERENCES

- [1] Halow, J S (1995), "Capacitance imaging of fluidized beds", in *Process Tomography: Principles, Techniques and Applications*, Eds Williams, R A, Beck, M S
- [2] Halow, J S, Boyle, E J, Daw, C S & Finney, C E A (1998), "PC-based, near-real-time, 3-dimensional simulation of fluidized beds", *Fluidization 9*, Durango, Co, USA, 541-548
- [3] Wang, S J, Dyakowski, T, Xie, C G, Williams R A & Beck M S (1995), "Real time capacitance imaging of bubble formation at the distributor of a fluidized bed", *Chemical Engineering Journal* 56(3), 95-100
- [4] White, R B (1996), "The characterisation of dense-phase fluidisation using capacitance tomographic imaging", *CFB5 proceedings*, MI1
- [5] Mathers, B J & Rhodes, M J (1996), "Use of process tomography to study the structure of a gas-solid fluidized bed", *Chemeca '96*, Vol 5, 57-62
- [6] Rhodes, M J, Sollaart, M & Wang X S (1998), "Structure of the dense-dilute interface in fast fluidization", *Fluidization 9*, Durango, Co, USA, 141-148
- [7] White, R B (1999), "Gas-solid contact efficiency in fluidised beds", PhD thesis, University of Melbourne, In preparation
- [8] Kunii, D & Levenspiel, O (1990), *Fluidization Engineering*, Second Edition, Butterworth-Heinemann
- [9] White, R B & Zakhari, A (1999), "Characterisation of flow regimes in the base of a cfb riser", submitted to CFB6
- [10] Geldart, D (1973), "Types of gas fluidisation", *Powder Technology* 7, 285 - 292
- [11] White, R B & Zakhari, A (1998), "Lateral mixing in a 1.56 m diameter cold fluid bed model", *Fluidization 9*, Durango, Co, USA, 349-356
- [12] Gilbertson, M A & Yates, Y G (1998), "The bubble bursting: the effect of pressure on a jet of bubbles in a fluidized bed", *World congress on particle technology 3*, paper 208

### Bed Fraction Profiles : Smelter Grade Alumina in a 200 mm ID Fluid Bed 400 mm deep bed, 12 sensors centred 200 mm above distributor

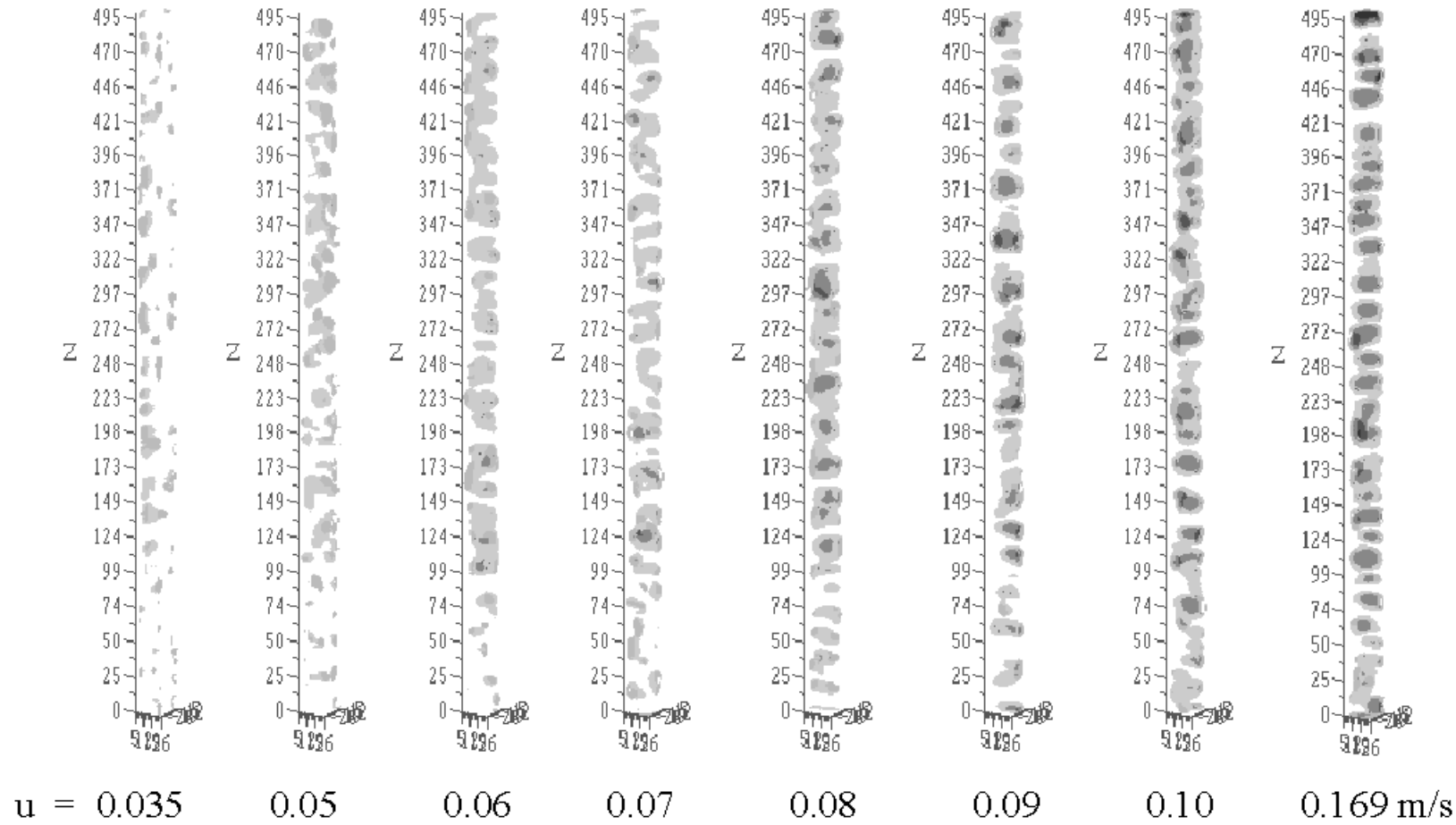


Figure 1: Bed fraction profile for 200 mm ID fluid bed with 400 mm deep bed of smelter grade alumina

## Bed Fraction Profiles : Smelter Grade Alumina in a 300 mm ID Fluid Bed 600 mm deep bed, 12 sensors centred 300 mm above distributor

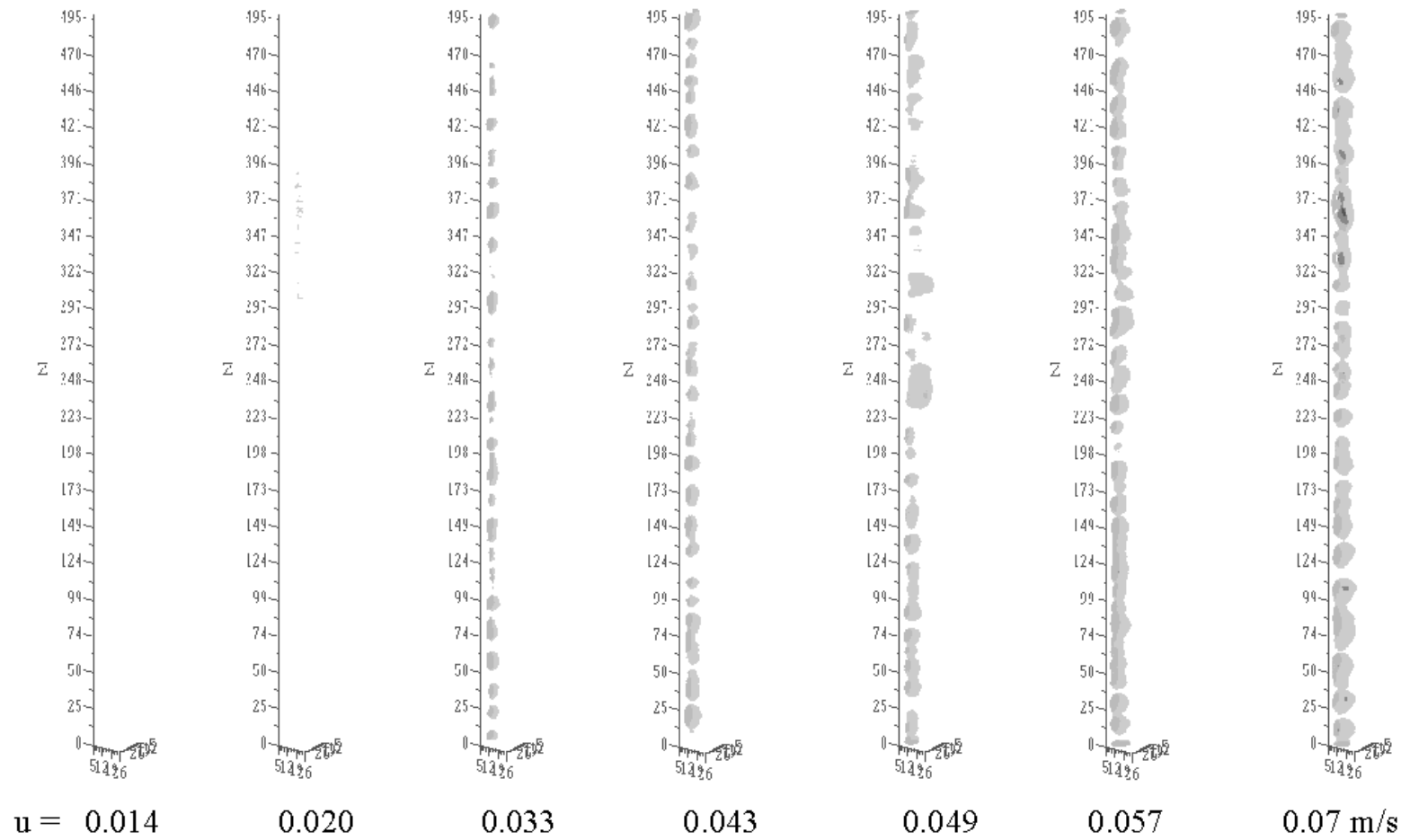


Figure 2: Bed fraction profile for 300 mm ID fluid bed with 600 mm deep bed of smelter grade alumina

### Bed Fraction Profiles : Smelter Grade Alumina in a 600 mm ID Fluid Bed 600 mm deep bed, 8 sensors centred 300 mm above distributor

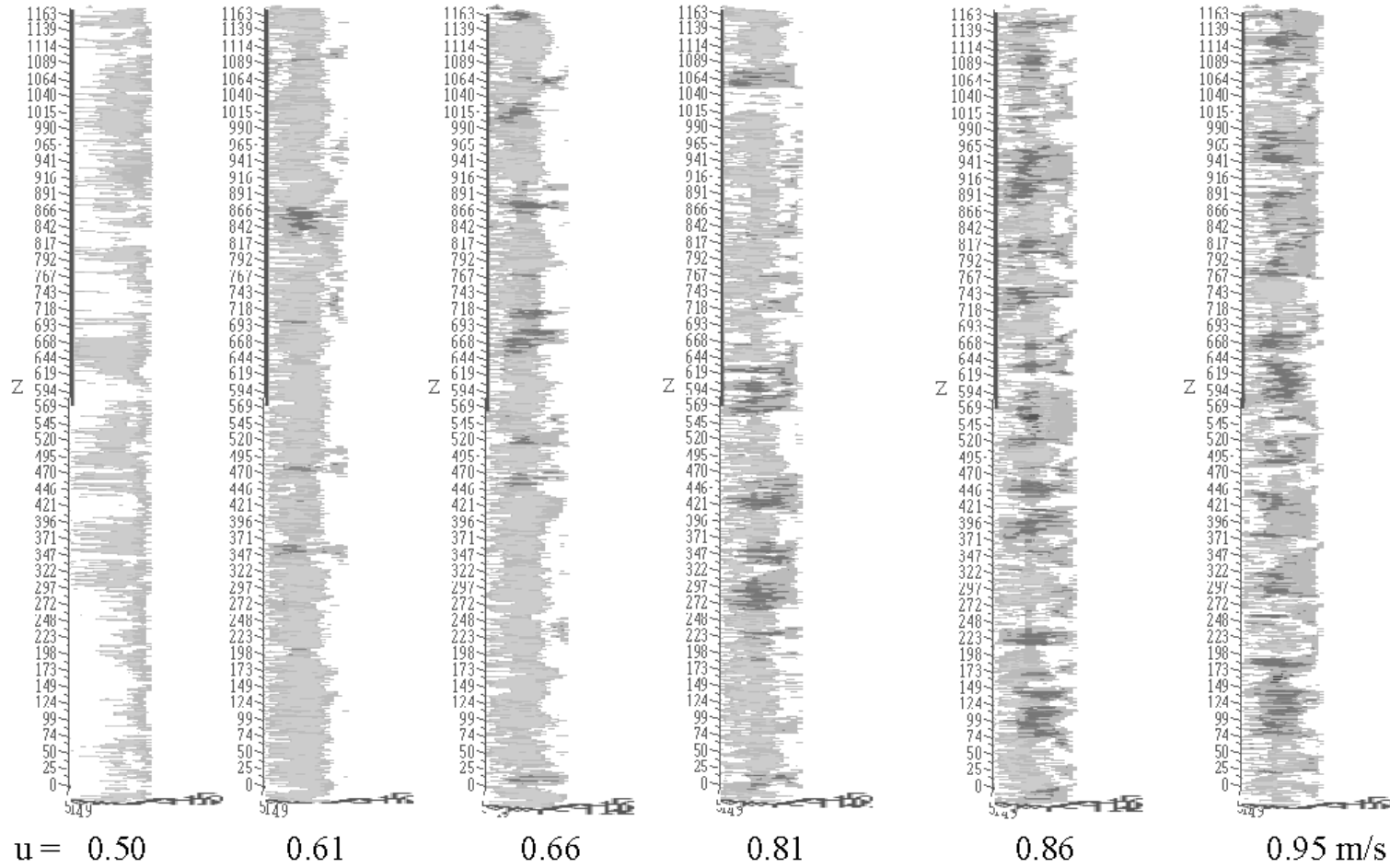


Figure 3: Bed fraction profile for 600 mm ID fluid bed with 600 mm deep bed of smelter grade alumina

### Bed Fraction Profiles : Smelter Grade Alumina in a 200 mm ID Fluid Bed 600 mm deep bed, 12 sensors centred 400 mm above distributor

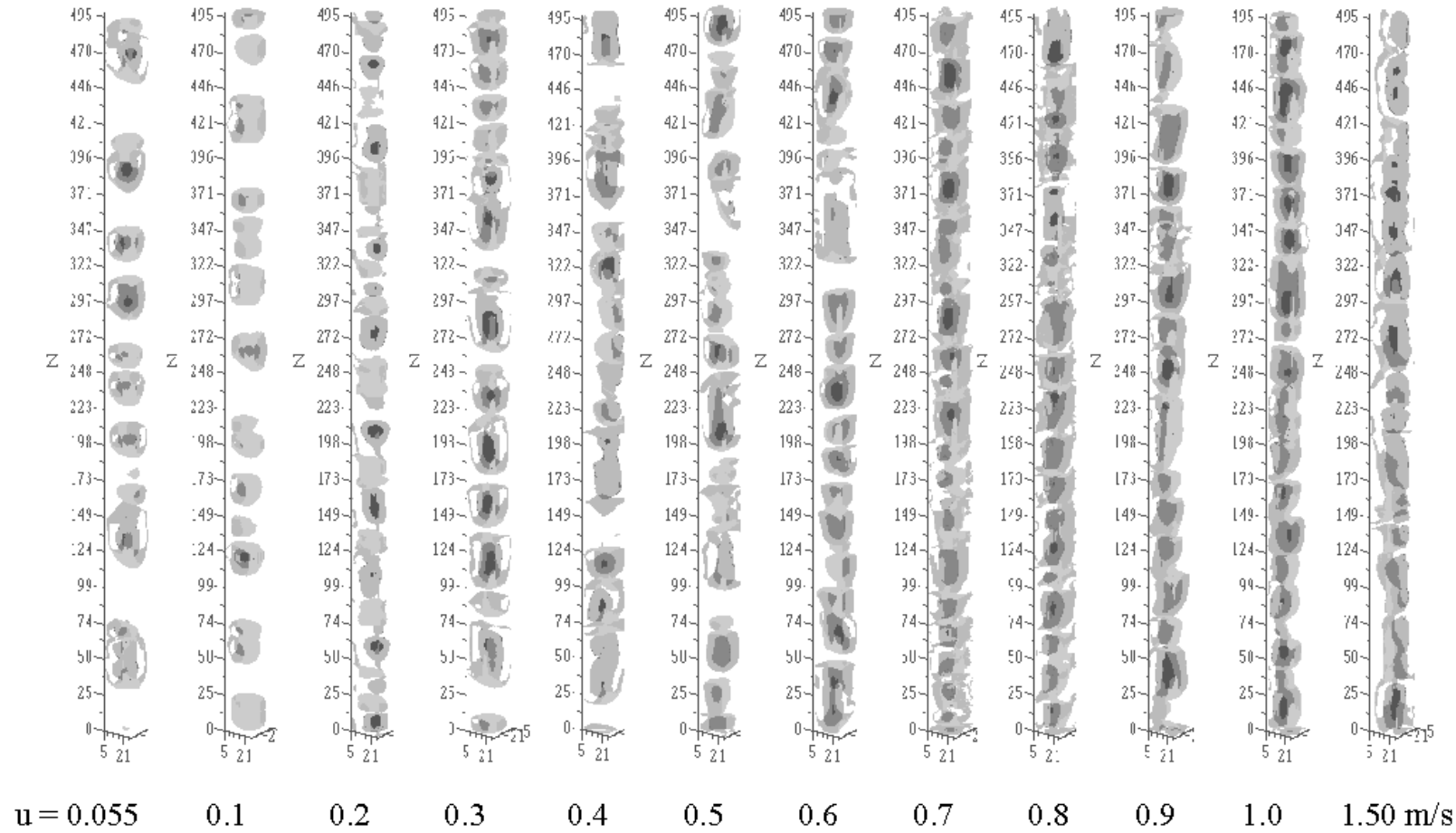


Figure 4: Bed fraction profile for 200 mm ID fluid bed with 600 mm deep bed of smelter grade alumina